Journal of Russian Laser Research, Volume 34, Number 2, March, 2013

QUANTIFICATION OF MIXED-STATE ENTANGLEMENT IN A QUANTUM SYSTEM INTERACTING WITH TWO TIME-DEPENDENT LASERS

Rasim Dermez[1,2]

[1] *Department of Physics*
Afyon Kocatepe University
Afyonkarahisar, 03200 Turkey
[2] *Department of Electrical and Computer Engineering*
Michigan Technological University
Houghton, Michigan, 49931 USA
E-mail: dermez @ aku.edu.tr

Abstract

We give a theoretical description of two time-dependent laser beams in the Λ scheme using a unitary transformation method and a trapped three-level ion. We extend earlier investigations aimed at finding the three types of density matrices. We present figures showing that the entanglement degree accelerates due to the time-dependent interaction and the second-order terms of the Lamb–Dicke parameter $\eta(t)$. Our results explain that the time-dependent ionic–phononic quantum system is observed at a higher degree of entanglement for three optimum times; these are, respectively, 16.5, 110, and 220 fs. These optimum entangled states can be modified for the structure of black holes in a probabilistic Universe.

Keywords: mixed-state entanglement, unitary transformation method, two time-dependent laser beams, weak excitation regime.

1. Introduction

The dynamics of trapped ions have been shown to produce a measurement of the states of macroscopic quantum systems [1,2]. Quantum information processing depends on various quantum physical phenomena, among which entanglement has been considered as one of the most significant properties. The effects between time-independent and time-dependent interactions have been discussed in connection with entanglement of trapped three-level ions [3]. Measurements on an entangled composite system cannot be explained in terms of classical correlations. Nonclassical correlations have been found in the Einstein, Podolsky, and Rosen (EPR) paradox [4], which are related to the Bell theorem [5]. It is important to point out that further insights into the dynamics of multilevel systems may be helpful in developing quantum information theory (QIT) [6]. The experimental achievements of QIT required such concepts as "quantum reality" and "counter part" which are mentioned in the EPR article.

The field of quantum communication leads to a variety of methods of bipartite entanglement [7] and to numerical calculations of the mixed-state entanglement of the time-dependent field and the trapped-ion

Manuscript submitted by the authors in English first on February 4, 2013 and in final form on March 30, 2013.
 1071-2836/13/3402-0192

system [8]. This field has been devoted to the quantification of the nonlocal effects of the bipartite mixed state [9]. Different aspects of entanglement have been discussed for one- or two-qubit systems [10–14]. Also, the quantum correlations including entanglement and discord with its geometric measure and classical correlations are studied for a bipartite partition of an open or closed quantum systems [15–18].

On the other hand, entangled pure states can be modeled physically by time-independent lasers and trapped three-level ions [19, 20]. The measure of the distinct characteristic of the global entanglement can provide a sufficient and necessary condition of full separability for pure states and conveniently extends to mixed states by minimizing the convex hull [21]. In addition, entangled states in second-order corrections can help to answer some important questions about quantum nonlinearity [22]. Using a simplified expression of concurrence in the Wootters measure of entanglement, Berrada et al. [23] examined the case of pure and mixed states of a two-qubit system based on the spin coherent states. With linear entropy as a measure of quantum entanglement, others have described the entanglement generated via a beam splitter using deformed Barut–Girardello coherent states [24]. Previous studies have also generated non-Gaussian entanglement from nonclassical photon statistics [25]. Also, polygamy of entanglement in multipartite quantum systems was studied by J. S. Kim [26]. An unknown mixed state was then studied which completely depends on the entanglement degree of the entangled mixed state as a resource [27]. An atom–field bipartite system in mixed state was employed to explain the partial entropy change and the entanglement in a cavity filled with the Kerr medium [28].

All the previous studies have been applied to the case of quantum entanglement. Therefore, in order to better understand long surviving states and black holes, we believe that the effects of the entanglement measurements in the quantum system are worthy of further investigation. If the gravitational effects are properly included, the entangled system behaves like a black hole [29]. It is found culminating in a classification of four-qubit entanglement from the physics of black holes [30]. Quantum superposition is supremely important, as Borsten expresses in a fundamentally probabilistic Universe [30].

We derive the entanglement degree from the eigenvalues of the atomic, the eigenvalues of the phononic, and the eigenvalues of the total system density matrices for mixed states. Here, there are three types of eigenvalues. The effects of the second-order terms of the Lamb–Dicke parameter (LDP) and the interactions of two time-dependent lasers increase the entanglement in the ionic–phononic quantum system. In our model, two coupling parameters LDP $\eta(t)$ and Rabi frequency $\Omega(t)$ are time-dependent for our system. We plotted entanglement in time and entanglement in space for the time-dependent ionic-phononic quantum system.

This paper is organized as follows.

In Sec. 2, the framework of the physical model of the time-dependent ionic-phononic quantum system is introduced. We describe the mixed-state entanglement and discuss the figures in Sec. 3. Finally, we present the concluding remarks in Sec. 4.

2. The Framework of the Physical Model of the Time-Dependent Ionic–Phononic Quantum System

Recently, quantum optics experiments operated beyond the LDP where $\eta < 1$ [31]. We consider a trapped three-level ion interacting with two time-dependent lasers. The time-dependent harmonic trap frequency $\nu(t)$ is the same for all levels of the trapped ion. We introduce the annihilation a and creation $a^\dagger$ operators of the vibrational phonons such that $a = \left[m\nu(t)/2\hbar\right]^{1/2}\left[x_{\text{ion}} + ip/m\nu(t)\right]$ and m is the mass

of the trapped ion. The total Hamiltonian for the time-dependent ionic-phononic quantum system is $H(t) = H_{\rm ion}(t) + H_1(t) + H_2(t)$. The trapped ion Hamiltonian $H_{\rm ion}(t)$ and the interacting Hamiltonians $H_1(t)$ and $H_2(t)$ are given as ($\hbar = 1$)

$$H_{\rm ion}(t) = \frac{p^2}{2m} + \frac{1}{2}m\nu^2(t)x_{\rm ion}^2 + \omega_{eg}|e\rangle\langle e|, \quad (1)$$

$$H_1(t) = \frac{\Omega_1(t)}{2}{\rm e}^{i(k_1 x_{\rm ion} - \omega_1 t)}|e\rangle\langle g| + {\rm h.c.}, \quad (2)$$

$$H_2(t) = \frac{\Omega_2(t)}{2}{\rm e}^{i(-k_2 x_{\rm ion} - \omega_2 t)}|e\rangle\langle r| + {\rm h.c.}, \quad (3)$$

where $x_{\rm ion}$ and p are the position and momentum of the center-of-mass of the trapped ion, respectively, and $|g\rangle$ corresponds to the ground level, $|r\rangle$ to the Raman level, and $|e\rangle$ to the excited level. Two time-dependent laser beams are characterized by their frequencies ω_1 and ω_2. We take $\omega = \omega_1 = \omega_2$. The time-dependent Rabi frequencies are $\Omega(t) = \Omega_1(t) = \Omega_2(t)$ (see Fig. 1).

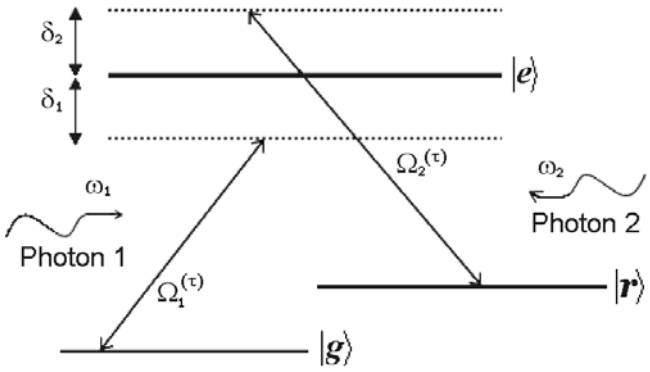

Fig. 1. A trapped three-level ion interacting with two time-dependent laser beams. The taken parameters are $\Omega(t) = \Omega_1(t) = \Omega_2(t)$, $\omega = \omega_1 = \omega_2$, $\delta = \delta_1 = \delta_2$ $\omega_1 = \omega_{eg} - \delta_1$, and $\omega_2 = \omega_{eg} - \delta_2$.

In quantum mechanics, the ionic center-of-mass motion can be represented by the standard harmonic-oscillator quantization of $H_{\rm ion}(t)$ with respect to $x_{\rm ion} = \sqrt{(1/2)m\nu(t)}\,(a^\dagger + a)$ and $p = i\sqrt{(1/2)m\nu(t)}\,(a^\dagger - a)$. Both time-dependent lasers of wavelength λ under consideration are slightly red detuned by the same amount $\delta = \nu(t)\eta^2(t)$, so that $\omega = \omega_{eg} - \delta$, $\omega_1 = \omega_{eg} - \delta_1$, and $\omega_2 = \omega_{eg} - \delta_2$, with ω_{eg} being the resonance frequency of the e–g transition, $\eta(t) = k/\sqrt{2m\nu(t)}$ the time-dependent LDP, and $k = 2\pi/\lambda$. Additionally, the weak excitation regime is assumed to satisfy $\nu(t) = \Omega(t)/2$. The rotating frame transformation is applied by

$$U_0 = \exp\left(-i\omega t|e\rangle\langle e|\right). \quad (4)$$

In view of the rapidly growing time-dependent Rabi frequency $\Omega(t) = \sinh(\omega_{eg}t)$ [31], our analytical results below become almost precise, since we use the second-order terms of $\eta(t)$. The optical Λ scheme considered above is shown to be equivalent to a cascade Ξ scheme for the vibrational phonon transitions under the weak excitation regime. Under a unitary transformation, the transformation matrix U is given by [32]

$$U = \frac{1}{2}\begin{pmatrix} 0 & \sqrt{2} & \sqrt{2} \\ -\sqrt{2}D[\eta(t)] & D[\eta(t)] & -D[\eta(t)] \\ \sqrt{2}D[-\eta(t)] & D[-\eta(t)] & -D[-\eta(t)] \end{pmatrix}. \quad (5)$$

In this matrix, we represent the basis vectors as $\langle e| = (1,0,0)$, $\langle r| = (0,1,0)$, and $\langle g| = (0,0,1)$, and use the Glauber displacement operators $D(\eta) = \exp\left[i\eta(t)(a + a^\dagger)\right]$. Applying the unitary transformation method of [32], we obtain the transformed Hamiltonian $\tilde{H}(t) = U^\dagger H(t) U$ in the form $\tilde{H}(t) = \tilde{H}_0(t) + \tilde{V}(t)$,

where

$$\tilde{H}_0(t) = \frac{\Omega(t)}{2}a^\dagger a + \frac{\Omega(t)}{2}\eta^2(t) + \frac{\Omega(t)}{2}\big(|r\rangle\langle r| - |g\rangle\langle g|\big), \tag{6}$$

$$\tilde{V}(t) = -i\epsilon(t)\big(a^\dagger|e\rangle\langle r| - a^\dagger|g\rangle\langle e| + \text{h.c.}\big), \tag{7}$$

with $\epsilon(t) = \Omega(t)\eta(t)/2\sqrt{2}$. Here, the LDP and Rabi frequency are time-dependent, $\epsilon(t)$ is derived following [32], and $\mu = \nu\eta/\sqrt{2}$ [32]. The three physical quantities are time-independent. This Hamiltonian describes cascade-type transitions of the vibrational phonons. It should be noted that the Raman level and the excited level become the intermediate and upper levels of the cascade, which is shown in Fig. 1. Using Eqs. (4)–(7), we determine the time evolution of the initial state $|\psi(0)\rangle$ as

$$|\psi(t)\rangle = U_0^\dagger U e^{-\int i\tilde{H}_0(t)\,dt}K(t)U^\dagger|\psi(0)\rangle, \tag{8}$$

where $K(t)$ is the well-known time-dependent propagator for the cascade Hamiltonian [32], $\hbar = 1$, and $\exp\left[-\int i\tilde{H}_0(t)dt\right]$ is the interaction-picture transformation. The given state of the vibrational phonons and the ion evolve in the Ξ configuration according to the time-dependent propagator $K(t)$ in the interaction picture, which is given by [32]

$$K(t) = \begin{pmatrix} \cos[\Lambda(t)t] & -\epsilon(t)S(t)a^\dagger & -\epsilon(t)S(t)a \\ \epsilon(t)aS(t) & 1+\epsilon^2(t)aL(t)a^\dagger & \epsilon^2(t)aL(t)a \\ \epsilon(t)a^\dagger S(t) & \epsilon^2(t)a^\dagger L(t)a^\dagger & 1+\epsilon^2(t)a^\dagger L(t)a \end{pmatrix}, \tag{9}$$

where $\Lambda(t) = \epsilon(t)\sqrt{2a^\dagger a + 1}$, $L(t) = \cos[\Lambda(t)t] - 1/\Lambda^2(t)$, and $S(t) = \sin[\Lambda(t)t]/\Lambda(t)$. The time-dependent ionic–phononic quantum state is transformed to an initial separable state of the cascade,

$$|\psi_K(t)\rangle = |\tilde{\psi}(0)\rangle = U^\dagger|\psi(0)\rangle = \sum_{ip}(M_{ip}(t)|\mathrm{i},p\rangle), \tag{10}$$

where i stands for the ionic state (e,r,g) and p stands for the phononic vibrational number $(0,1,2,3)$. Applying the time-dependent propagator $K(t)$ to the initial separable state of the cascade, we obtained the ionic–phononic quantum state $|\psi_K(t)\rangle = \sum_{ip}(M_{ip}(t)|\mathrm{i},p\rangle)$.

In the second-order terms of $\eta(t)$, the significant coefficients of $|\psi_K(t)\rangle$ become

$$\begin{aligned}
M_{e0}(t) &= \exp\big[-i\sigma(t)\eta(t)\big]\big\{\sqrt{1/2}(x+\sqrt{1-x^2})\cos\big[\sqrt{1/2}\sigma(t)\big] + (x-\sqrt{1-x^2})/2\sin\big[\sqrt{1/2}\sigma(t)\big]\alpha \\
&\quad +2^{-1}i\big[(x+\sqrt{1-x^2})\sin\big[\sqrt{1/2}\sigma(t)\big]\eta(t) - \big[(-x+\sqrt{1-x^2})\cos[\sqrt{1/2}\sigma(t)]\alpha\sqrt{2}\eta(t)\big]\big\}, \\
M_{e1}(t) &= \exp\big\{-i\sigma(t)[1/\eta(t)+\eta(t)]\big\}\big[2^{-1}\cdot 3^{-1/2}(-x+\sqrt{1-x^2})\sin\big[\sqrt{3/2}\sigma(t)\big] \\
&\quad +\sqrt{1/2}\big\{(x+\sqrt{1-x^2})\,\cos\big[\sqrt{3/2}\sigma(t)\big]\big\}\alpha + \sqrt{1/2}i(x-\sqrt{1-x^2}) \\
&\quad \times\cos\big[\sqrt{3/2}\sigma(t)\big]\eta(t) + 2^{-1}\cdot 3^{-1/2}\big(ix+i\sqrt{1-x^2}\big)\sin[\sqrt{3/2}\sigma(t)]\alpha\eta(t)\big], \\
M_{e2}(t) &= \exp\big\{-i\sigma(t)[2/\eta(t)+\eta(t)]\big\}\big[10^{-1/2}\big[(-x+\sqrt{1-x^2})\sin\big[\sqrt{5/2}\sigma(t)\big]\alpha\big] \\
&\quad -\big\{10^{-1/2}\big(i(x+\sqrt{1-x^2})\sin\big[\sqrt{5/2}\sigma(t)\big]\big\} + i(-x+\sqrt{1-x^2})\cos[\sqrt{5/2}\sigma(t)]\alpha\big)\eta(t)\big], \\
M_{e3}(t) &= \exp\big\{-i\sigma(t)[3/\eta(t)+\eta(t)]\big\}\big(\sqrt{3/14}ix + i\sqrt{1-x^2}\big)\sin\big[\sqrt{7/2}\sigma(t)\big]\alpha\eta(t),
\end{aligned}$$

$$
\begin{aligned}
M_{r0}(t) &= \exp\{-i\sigma(t)[1/\eta(t)+\eta(t)]\}\Big\{6^{-1}(x-\sqrt{1-x^2})\big(2+\cos\big[\sqrt{3/2}\sigma(t)\big]\big)\\
&+6^{-1/2}\big\{(x+\sqrt{1-x^2})\sin\big[\sqrt{3/2}\sigma(t)\big]\alpha+i(x-\sqrt{1-x^2})\sin\big[\sqrt{3/2}\sigma(t)\big]\big\}\eta\\
&+\big((2i/3)(x+\sqrt{1-x^2})+6^{-1}\big(-ix-i\sqrt{1-x^2}\big)\cos\big[\sqrt{3/2}\sigma(t)\big]\big)\alpha\eta(t)\Big\},\\
M_{r1}(t) &= \exp\{-i\sigma(t)[2/\eta(t)+\eta(t)]\}\Big[10^{-1}\cdot(x-\sqrt{1-x^2})\big(-3-2\cos\big[\sqrt{5/2}\sigma(t)\big]\big)\alpha\\
&+i\cdot 10^{-1}(x+\sqrt{1-x^2})\big(3+2\cos\big[\sqrt{5/2}\sigma(t)\big]\big)\eta(t)-i\sqrt{2/5}(-x+\sqrt{1-x^2})\sin[\sqrt{5/2}\sigma(t)]\alpha\eta(t)\Big],\\
M_{r2}(t) &= \exp\{-i\sigma(t)[3/\eta(t)+\eta(t)]\}\cdot 7\cdot 2^{-1/2}i(x+\sqrt{1-x^2})\big(4+3\cos\big[\sqrt{7/2}\sigma(t)\big]\big)\alpha\eta(t),\\
M_{g0}(t) &= \exp\big\{-i\sigma(t)[-1/\eta(t)+\eta(t)]\big\}\cdot 2^{-1}\big(-(x-\sqrt{1-x^2})-i(x+\sqrt{1-x^2})\alpha\eta(t)\big),\\
M_{g1}(t) &= \exp\big[-i\sigma(t)\eta(t)\big]\Big[2^{-1/2}(x+\sqrt{1-x^2})\sin\big[\sqrt{1/2}\sigma(t)\big]+2^{-1}\Big\{(-x+\sqrt{1-x^2})\\
&\times\cos\big[\sqrt{1/2}\sigma(t)\big]\alpha-i(x+\sqrt{1-x^2})\cos\big[\sqrt{1/2}\sigma(t)\big]\eta(t)\Big\}-2^{-1/2}i(-x+\sqrt{1-x^2})\\
&\times\sin[\sqrt{1/2}\sigma(t)]\alpha\eta(t)\Big],\\
M_{g2}(t) &= \exp\big\{-i\sigma(t)[1/\eta(t)+\eta(t)]\big\}\Big[3^{-1}\cdot 2^{-1/2}(x-\sqrt{1-x^2})\big(1-\cos\big(\sqrt{3/2}t\big)\big)\\
&+3^{-1/2}\big\{(x+\sqrt{1-x^2})\sin\big(\sqrt{3/2}t\big)\alpha+i(x-\sqrt{1-x^2})\sin\big(\sqrt{3/2}t\big)\eta(t)\big\}\\
&-3^{-1}i(x+\sqrt{1-x^2})(2^{-1}+2^{-1/2})\cos(\sqrt{3/2}t)\alpha\eta(t)\Big],\\
M_{g3}(t) &= \exp\{-i\sigma(t)[2/\eta(t)+\eta(t)]\}50^{-1}\sqrt{3}\Big[(x-\sqrt{1-x^2})\big(-1+\cos\big[\sqrt{5/2}\sigma(t)\big]\big)\alpha\\
&+i(x+\sqrt{1-x^2})\big(-1+\cos\big[\sqrt{5/2}\sigma(t)\big]\big)\eta(t)-10^{-1/2}i(-x+\sqrt{1-x^2})\sin[\sqrt{5/2}\sigma(t)]\alpha\eta(t)\Big].
\end{aligned}
$$

In the above equations, $M_{r3}(t)=0$, $\sigma(t)=\nu(t)\eta(t)t$, and x are the probability amplitudes of the trapped ion. According to the time evolution in Eq. (8), the final ionic–phononic quantum state of the system can be written as

$$
|\psi(t)\rangle=\sum_{n=0}^{3}\big(A_{en}(t)|e,n\rangle+B_{rn}(t)|r,n\rangle+C_{gn}(t)|g,n\rangle\big). \tag{11}
$$

In our calculations, we used $|e_0\rangle,|e_1\rangle,|e_2\rangle,|e_3\rangle$, $|r_0\rangle,|r_1\rangle,|r_2\rangle,|r_3\rangle$, and $|g_0\rangle,|g_1\rangle,|g_2\rangle,|g_3\rangle$ to obtain the evolution of the density matrix of the time-dependent ionic–phononic system.

For the quantum system, significant functions of Eq. (11) are written as

$$
\begin{aligned}
&A_{e0(t)}=\sqrt{1/2}\mathrm{e}^{-i\omega t}\mathrm{e}^{-2iN(t)}[M_{r0}(t)+M_{g0}(t)],\quad A_{e1(t)}=\sqrt{1/2}\mathrm{e}^{-i\omega t}\mathrm{e}^{-2iN(t)}[M_{r1}(t)+M_{g1}(t)],\\
&A_{e2(t)}=\sqrt{1/2}\mathrm{e}^{-i\omega t}\mathrm{e}^{iN(t)}[M_{r2}(t)+M_{g2}(t)],\quad A_{e3(t)}=\sqrt{1/2}\mathrm{e}^{-i\omega t}\mathrm{e}^{2iN(t)}[M_{r3}(t)+M_{g3}(t)],\\
&B_{r0}(t)=\mathrm{e}^{-iN(t)}\Big[-\frac{M_{e0}(t)}{\sqrt{2}}+\frac{M_{r0}(t)-M_{g0}(t)}{2}\Big]+i\eta(t)\mathrm{e}^{-2iN(t)}\Big[-\frac{M_{e1}(t)}{\sqrt{2}}+\frac{M_{r1}(t)-M_{g1}(t)}{2}\Big],\\
&B_{r1}(t)=i\eta(t)\mathrm{e}^{-iN(t)}\Big[-\frac{M_{e0}(t)}{\sqrt{2}}+\frac{M_{r0}(t)-M_{g0}(t)}{2}\Big]+\mathrm{e}^{-iN(t)}\Big[\frac{-M_{e1}(t)}{\sqrt{2}}+\frac{M_{r1}(t)-M_{g1}(t)}{2}\Big]\\
&\quad+\sqrt{2}i\eta(t)\mathrm{e}^{iN(t)}\Big[-\frac{M_{e2}(t)}{\sqrt{2}}+\frac{M_{r2}(t)-M_{g2}(t)}{2}\Big],
\end{aligned}
$$

$$B_{r2}(t)=\sqrt{2}i\eta(t)\mathrm{e}^{-2iN(t)}\Big[-\frac{M_{e1}(t)}{\sqrt{2}}+\frac{M_{r1}(t)-M_{g1}(t)}{2}\Big]+\mathrm{e}^{iN(t)}\Big[-\frac{M_{e2}(t)}{\sqrt{2}}+\frac{M_{r2}(t)-M_{g2}(t)}{2}\Big]$$
$$+\sqrt{3}i\eta(t)\mathrm{e}^{-2iN(t)}\Big[-\frac{M_{e3}(t)}{\sqrt{2}}-\frac{M_{g3}(t)}{2}\Big],$$
$$B_{r3}(t)=\sqrt{3}i\eta(t)\mathrm{e}^{-2iN(t)}\Big[-\frac{M_{e2}(t)}{\sqrt{2}}+\frac{M_{r2}(t)-M_{g2}(t)}{2}\Big]+\mathrm{e}^{iN(t)}\Big[\frac{M_{e3}(t)}{\sqrt{2}}+\frac{M_{g3}(t)}{2}\Big],$$

$$C_{g0}(t)=\mathrm{e}^{-2iN(t)}\Big[\frac{M_{e0}(t)}{\sqrt{2}}+\frac{M_{r0}(t)-M_{g0}(t)}{2}\Big]+-i\eta(t)\mathrm{e}^{iN(t)}\Big[\frac{M_{e1}(t)}{\sqrt{2}}+\frac{M_{r1}(t)-M_{g1}(t)}{2}\Big],$$
$$C_{g1}(t)=-i\eta(t)\mathrm{e}^{-2iN(t)}\Big[\frac{M_{e0}(t)}{\sqrt{2}}+\frac{M_{r0}(t)-M_{g0}(t)}{2}\Big]+\mathrm{e}^{iN(t)}\Big[-\frac{M_{e1}(t)}{\sqrt{2}}+\frac{M_{r1}(t)-M_{g1}(t)}{2}\Big]$$
$$-\sqrt{2}i\eta(t)\mathrm{e}^{-2iN(t)}[M_{e2}(t)/\sqrt{2}+\frac{M_{r2}(t)-M_{g2}(t)}{2}\Big],$$
$$C_{g2}(t)=-\sqrt{2}i\eta(t)\mathrm{e}^{iN(t)}\Big[\frac{M_{e1}(t)}{\sqrt{2}}+\frac{M_{r1}(t)-M_{g1}(t)}{2}\Big]+\mathrm{e}^{iN(t)}\Big[-\frac{M_{e2}(t)}{\sqrt{2}}+\frac{M_{r2}(t)-M_{g2}(t)}{2}\Big]$$
$$+\sqrt{3}i\eta(t)\mathrm{e}^{-2iN(t)}\Big[\frac{M_{e3}(t)}{\sqrt{2}}-\frac{M_{g3}(t)}{2}\Big],$$
$$C_{g3}(t)=-\sqrt{3}i\eta(t)\mathrm{e}^{iN(t)}\Big[\frac{M_{e2}(t)}{\sqrt{2}}+\frac{M_{r2}(t)-M_{g2}(t)}{2}\Big]+\mathrm{e}^{iN(t)}\Big[\frac{M_{e3}(t)}{\sqrt{2}}-\frac{M_{g3}(t)}{2}\Big].$$

With the above equations, $\omega=\omega_{eg}-\eta^2(t)\nu(t)$ and $N(t)=\int\nu(t)\,dt=\int\Omega(t)/2\,dt=\cosh(\omega_{eg}t)/2\omega_{eg}$.

3. Mixed-State Entanglement

The quantum correlations between the internal degrees of freedom of the ion with the external degrees of freedom may lead to quantum-entangled-state formations, which cannot be generated by local operations in corresponding Hilbert spaces of constituent subsystems of the composite system. Mixed-state entanglement achieved in the previous section evolves in the Hilbert space $\mathbf{H}=\mathbf{H}_{\mathrm{i}}\otimes\mathbf{H}_p$ of dimension 3×4. Two entangled pure states can result in quantum entanglement much less than the average mixed state entanglement. The initial state of the trapped three-level ion is written as

$$\rho^{\mathrm{ion}}(0)=x^2|g\rangle\langle g|+(-\sqrt{1-x^2})^2|r\rangle\langle r|=\begin{pmatrix}0&0&0\\0&x^2&0\\0&0&(1-x^2)\end{pmatrix},\tag{12}$$

where the normalization condition is $1=x^2+(1-x^2)$.

In view of the second-order terms of $\eta(t)$, this initial state determines a state of vibrational phonons that is approximately normalized. Also, let the initial state of the phonon be written as

$$\rho^{\mathrm{phonon}}(0)=(|0\rangle+\alpha|1\rangle)\otimes(\langle 0|+\alpha^*\langle 1|).\tag{13}$$

With the unitary transformation method, the total density matrix of the ionic–phononic quantum system is given by

$$\rho_{\mathrm{i}-p}(t)=U^{\dagger}(t)[\rho^{\mathrm{ion}}(0)\otimes\rho^{\mathrm{phonon}}(0)]U(t).\tag{14}$$

In this way, we will deal exclusively with the mixed-state entanglement. Therefore, from Eq. (14), the von Neumann entropy of the time-dependent ionic–phononic quantum system is described as [33–36]

$$S(\rho_{\mathrm{i}-p}) = \sum_{\mathrm{i}=1}^{12} \lambda_{\mathrm{i}}^{\mathrm{i}-p} \log(\lambda_{\mathrm{i}}^{\mathrm{i}-p}). \tag{15}$$

By tracing over the phononic variable, we obtain a 3×3 reduced density matrix ρ_{i} of the ion, such that

$$\rho_{\mathrm{ion}} = \mathrm{Tr}_{\mathrm{phonon}}(\rho_{\mathrm{i}-p}) = \begin{pmatrix} \mathrm{Tr}\,|u\rangle\langle u| & \mathrm{Tr}\,|u\rangle\langle v| & \mathrm{Tr}\,|u\rangle\langle w| \\ \mathrm{Tr}\,|v\rangle\langle u| & \mathrm{Tr}\,|v\rangle\langle v| & \mathrm{Tr}\,|v\rangle\langle w| \\ \mathrm{Tr}\,|w\rangle\langle u| & \mathrm{Tr}\,|w\rangle\langle v| & \mathrm{Tr}\,|w\rangle\langle w| \end{pmatrix}, \tag{16}$$

where $|u\rangle\langle u|$ is a 4×4 matrix.

By tracing over the ionic variable, we take a 4×4 reduced density matrix ρ_p of the phonon, such that

$$\rho_{\mathrm{phonon}} = \mathrm{Tr}_{\mathrm{ion}}(\rho_{\mathrm{i}-p}) = \begin{pmatrix} \mathrm{Tr}\,|a\rangle\langle a| & \mathrm{Tr}\,|a\rangle\langle b| & \mathrm{Tr}\,|a\rangle\langle c| & \mathrm{Tr}\,|a\rangle\langle d| \\ \mathrm{Tr}\,|b\rangle\langle a| & \mathrm{Tr}\,|b\rangle\langle b| & \mathrm{Tr}\,|b\rangle\langle c| & \mathrm{Tr}\,|b\rangle\langle d| \\ \mathrm{Tr}\,|c\rangle\langle a| & \mathrm{Tr}\,|c\rangle\langle b| & \mathrm{Tr}\,|c\rangle\langle c| & \mathrm{Tr}\,|c\rangle\langle d| \\ \mathrm{Tr}\,|d\rangle\langle a| & \mathrm{Tr}\,|d\rangle\langle b| & \mathrm{Tr}\,|d\rangle\langle c| & \mathrm{Tr}\,|d\rangle\langle d| \end{pmatrix}. \tag{17}$$

where $|a\rangle\langle a|$ is a 3×3 matrix. Using the above equations, we write the final expression for the quantum entanglement degree for the time-dependent ionic–phononic quantum system as

$$E_{\mathrm{ent}}(\rho_{\mathrm{i}}, \rho_p) = -S(\rho_{\mathrm{ion}}) + S(\rho_{\mathrm{phonon}}) - S(\rho_{\mathrm{i}-p}). \tag{18}$$

With three types of eigenvalues, we can rewrite the quantum entanglement as a quantum measure

$$E_{\mathrm{ent}}(\rho_{\mathrm{i}}, \rho_p) = -\sum_{\mathrm{i}=1}^{3} \lambda_{\mathrm{i}}^{\mathrm{ion}} \log(\lambda_{\mathrm{i}}^{\mathrm{ion}}) + \sum_{\mathrm{i}=1}^{4} \lambda_{\mathrm{i}}^{\mathrm{phonon}} \log(\lambda_{\mathrm{i}}^{\mathrm{phonon}}) - \sum_{\mathrm{i}=1}^{12} \lambda_{\mathrm{i}}^{\mathrm{i}-p} \log(\lambda_{\mathrm{i}}^{\mathrm{i}-p}), \tag{19}$$

where $\lambda_{\mathrm{i}}^{\mathrm{ion}}$ are the eigenvalues of the ionic reduced density matrix, $\lambda_{\mathrm{i}}^{\mathrm{phonon}}$ are the eigenvalues of the phononic reduced density matrix, and $\lambda_{\mathrm{i}}^{\mathrm{i}-p}$ are the eigenvalues of the total density matrix of the ionic–phononic system. Equation (19) provides a measure of how well the entanglement between two subsystems is preserved in a quantum process.

We have constructed a theoretical description of the trapped three-level ion interacting with two time-dependent laser beams under the Λ scheme shown in Fig. 1. Our results are presented in the second-order terms of $\eta(t)$. The time-dependent Rabi frequency is $\Omega(t) = \sinh(\omega_{eg}t)$; the other parameters are $\omega_{eg} = 5 \cdot 10^{14}$ Hz, the time-dependent harmonic trap frequency $\nu(t) = \sinh(\omega_{eg}t)/2$, and $\alpha = 0.01$. The optimum probability amplitude of the trapped ion in Fig. 2 is $x = 1/\sqrt{2}$. Thus, the figures demonstrate also the significance of time-dependent ionic–phononic quantum state of Eq. (10).

The mixed-state entanglement reaches $E_{\mathrm{ent}} = 0.84$ for $x = 1/\sqrt{2}$ and within the quantum entanglement formula in Eq. (19). We found the optimum three times in Fig. 2. These optimum times are $t = 1.65 \cdot 10^{-14}$ s (16.5 fs), $t = 1.1 \cdot 10^{-13}$ s (110 fs), and $t = 2.2 \cdot 10^{-13}$ s (220 fs). It is seen that the time-dependent ionic–phononic quantum system stays in the mixed entangled state in the 16.5 fs region

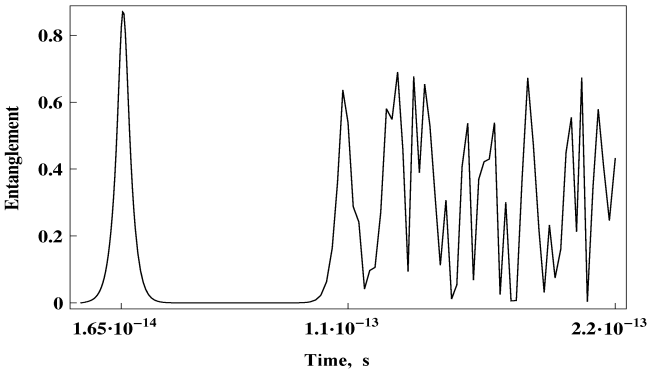

Fig. 2. The time evolution of the quantum entanglement of the ionic–phononic quantum system. The time-dependent harmonic trap frequency $\nu(t) = \sinh(\omega_{eg}t)/2$, Rabi frequency $\Omega(t) = \sinh(\omega_{eg}t)$, and the optimum probability amplitude $x = 1/\sqrt{2}$ are used with $\omega_{eg} = 5 \cdot 10^{14}$ Hz. The system is initially prepared in the states $\rho^{\text{ion}}(0) = x^2|g\rangle\langle g| + (1-x^2)|r\rangle\langle r|$ and $\rho^{\text{phonon}}(0) = (|0\rangle + \alpha|1\rangle) \otimes (\langle 0| + \alpha^*\langle 1|$ with $\alpha = 0.01$.

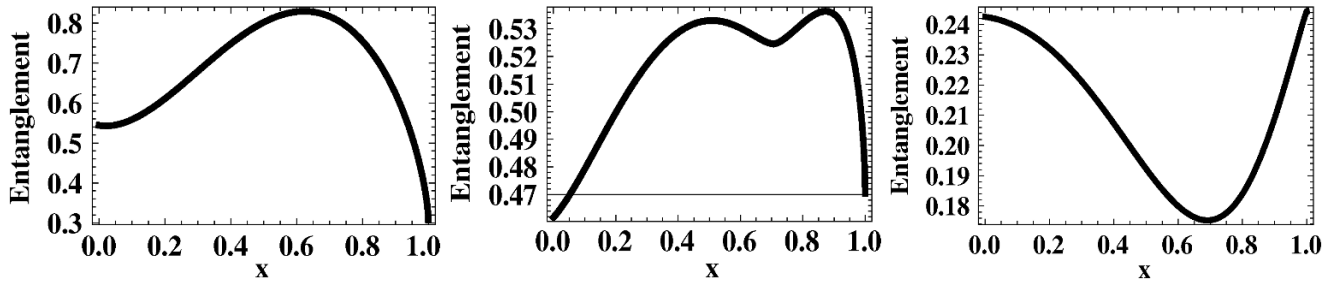

Fig. 3. The evolution of the probability amplitude x of the quantum entanglement of the ionic–phononic quantum system. The time-dependent harmonic trap frequency $\nu(t) = \sinh(\omega_{eg}t)/2$ and Rabi frequency $\Omega(t) = \sinh(\omega_{eg}t)$ are used with $\omega_{eg} = 5 \cdot 10^{14}$ Hz. For this system, these optimum times are $t = 1.65 \cdot 10^{-14}$ s (a), $t = 1.1 \cdot 10^{-13}$ s (b), and $t = 2.2 \cdot 10^{-13}$ s (c). The system is initially prepared in the states $\rho^{\text{ion}}(0) = x^2|g\rangle\langle g| + (1-x^2)|r\rangle\langle r|$ and $\rho^{\text{phonon}}(0) = (|0\rangle + \alpha|1\rangle) \otimes (\langle 0| + \alpha^*\langle 1|$ with $\alpha = 0.01$.

longer than it does in the 110 and 220 fs regions (see Fig. 2). Indeed, there are 14 dips of the quantum entanglement in this figure. In particular, the mixed-state entanglement of the system decreases from 0.84 to 0.70 across time in Fig. 2. We recorded entanglement while it was between $E_{\text{ent}} = 0 - 0.84$. For the quantum system, the mixed-state entanglement evolves while oscillating. This behavior is illustrated in Fig. 2.

The x evolution of the system is shown in Fig. 3. In the three curves in this figure, we elucidate the optimum probability amplitude of entanglement of the ionic–phononic quantum system for the optimum three times 16.5, 110, and 220 fs. We find that entanglement is maximum at $E_{\text{ent}} = 0.84$, while the optimum probability amplitude is $x = 1/\sqrt{2}$ (see Fig. 3 a). Similarly, it is minimum at $E_{\text{ent}} = 0$ while the optimum probability amplitude is $x = 1/\sqrt{2}$ (see Fig. 3 c). We see that the time-dependent interaction and $\eta(t)$ may enhance the degree of system entanglement.

Figure 4 demonstrates the time dependence of $\eta(t)$ and $\Omega(t)$ assuming $\hbar = 1$ in the ionic–phononic quantum system; $\eta(t) = k/\sqrt{2m\nu(t)}$ and $\Omega(t) = \sinh(\omega_{eg}t)$ are the time-dependent coupling parameters of the system. Figure 5 shows the time dependence of the Schmidt coefficients (SCs), which are the eigenvalues of the reduced density matrix in Eq. (16). The eigenvalues are the first term $\lambda_{\text{i}}^{\text{ion}}$ in Eq. (19), and the quantum-mechanical normalization is equal to $\lambda_1^{\text{ion}} + \lambda_2^{\text{ion}} + \lambda_3^{\text{ion}} = 1$ (see Fig. 5).

These figures and results are in parallel with our analytical observation. As a consequence, this observation conforms with [8, 35]. Correspondingly, our report agrees with experimental direct observation of the mixed state entanglement in [37].

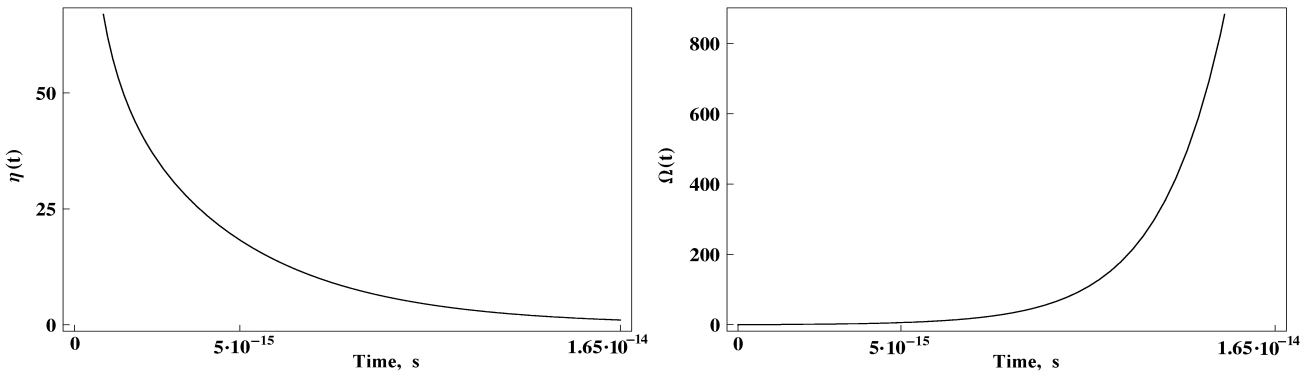

Fig. 4. The time dependences of scaled LDP $\eta(t)$ (left) and $\Omega(t)$ (right) in the ionic–phononic quantum system assuming $\hbar = 1$. The system is initially prepared in the states $\rho^{\rm ion}(0) = x^2|g\rangle\langle g| + (1-x^2)|r\rangle\langle r|$ and $\rho^{\rm phonon}(0) = (|0\rangle + \alpha|1\rangle) \otimes (\langle 0| + \alpha^*\langle 1|$ with $\alpha = 0.01$.

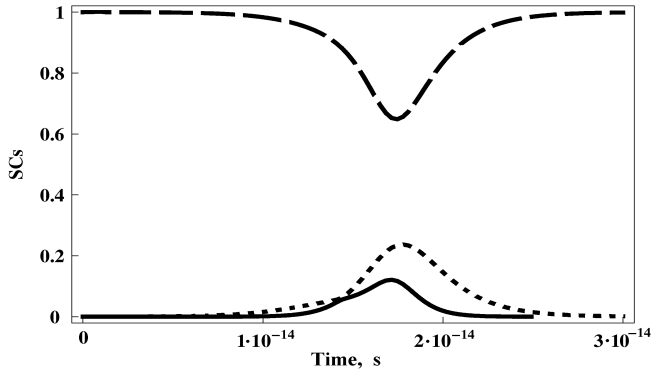

Fig. 5. The time dependence of SCs in the ionic–phononic quantum system (assuming $\hbar = 1$) shown for three eigenvalues of the first term in Eq. (19) for the ionic system Λ_1 by the solid curve, Λ_2 by the dashed curve, and Λ_3 by the dotted curve. The time-dependent harmonic trap frequency $\nu(t) = \sinh(\omega_{eg}t)/2$, the Rabi frequency $\Omega(t) = \sinh(\omega_{eg}t)$, and the optimum probability amplitude $x = 1/\sqrt{2}$ are used with $\omega_{eg} = 5 \cdot 10^{14}$ Hz. The system is initially prepared in the states $\rho^{\rm ion}(0) = x^2|g\rangle\langle g| + (1-x^2)|r\rangle\langle r|$ and $\rho^{\rm phonon}(0) = (|0\rangle + \alpha|1\rangle) \otimes (\langle 0| + \alpha^*\langle 1|)$ with $\alpha = 0.01$.

As we reported in our study, in a similar way that uses the reduced density matrix, the entanglement entropy is calculated in terms of the infinitesimal generator of conformal transformations that keep the sphere fixed [38]. The relation to the tomographic entropy associated to the spin-state tomograms was introduced in [39, 40].

Various proposals to construct two-component cat states in trapped two-level ion systems have been discussed extensively in recent years [41, 42]. The pure-state entanglement was obtained physically in quantum states of the time-independent three-level trapped ions [43]. Dermez et. al. [44] have investigated the quantum correlations of a fully-trapped ion interacting with two time-independent laser beams, in view of the LDP. In [44], each of the three probability amplitudes of the trapped ion was taken as $1/\sqrt{3}$.

4. Concluding Remarks

In conclusion, we considered the trapped-ion model with two time-dependent laser beams in the Λ scheme. In this study, we solved the time-dependent Hamiltonian of the ionic–phononic quantum system. We obtained an exact solution of the total density matrix $\rho_{{\rm i}-p}(t) = U^\dagger(t)[\rho^{\rm ion}(0) \otimes \rho^{\rm phonon}(0)]U(t)$. Analytic calculations under our theoretical conditions are characterized by the time dependence of the total-system Hamiltonian. Henceforth, there are two key points in this paper, namely, the time-dependent phononic state and the second-order terms of $\eta(t)$, both being revolved around the behavior of the mixed-state entanglement.

We demonstrated that the quantum entanglement is stored in the ionic–phononic system under con-

sideration. The nature of quantum entanglement is strongly related to time-dependent modulation. The highest degree of mixed state entanglement is $E_{ent} = 0.84$ with $t = 1.65 \cdot 10^{-14}$ s (1.65 fs) in Fig. 2. The maxima of the fourteen entanglement peaks are recorded in the time interval of 16.5 to 220 fs (see Fig. 2). Under the three optimum times 16.5, 110, and 220 fs, the evolution of the optimum probability amplitude $x = 1/\sqrt{2} = 0.707$ of the quantum system is shown in Fig. 3. As the entanglement evolves within these times, we see that its features correlate with the occupancy properties of the ionic–phononic system. Therefore, it is worth noting that the amount of mixed state entanglement is long-lived and very sensitive to $\eta(t)$.

The study of the physical properties of the ion–phonon interaction is an important topic in quantum optics. Our trapped three-level ionic–phononic system displays a very broad range of applications in quantum optics and quantum information. As a consequence of these applications, it can be found that the mixed-state entanglement highly depends on $\eta(t)$. Our results can be experimentally realized with the designed time-dependent coupling parameters $\eta(t)$ and $\Omega(t)$. The results reported in this paper are compatible with previous studies.

Punch-line result: That the value of the maximally entangled state is 0.84 (a), and that the ionic–phononic quantum system is time-dependent (b) are the two main extractions that are most significant among the many results of this article. For the modification of black holes, the time-dependent ionic–phononic quantum system is a very unique example. Also, the amount of mixed-state entanglement is long-lived in Fig. 3. Therefore, the long survival value of entanglement in the system is very handy and useful, in understanding the structure of black holes. Entangled atomic-size systems ignore the mass attraction and do not take into account the gravity. If the quantum entanglement in the gravitational field involves following mathematical formulas, the quantum entangled state acts as a black hole. The time-dependent ionic–phononic quantum system is more useful than our time-independent system employed also in other studies, because, in this quantum system, the amount of entanglement and its long survival are improved in comparison with other studies.

In the future, we hope that the optimum times and the long-survival entangled states can be useful for understanding black holes. Then, the quantum entanglement system can behave like the black hole. Accordingly, trapped ions and the vibrational phonons can be modified in applied physics. Generalizing previous results, pure- and mixed-state entanglement degrees provide a long-lived entangled state because of quantum correlations. Eventually, we expect our study to be helpful for analyzing the system mixed-state entanglement in practical applications.

Acknowledgments

This work was supported by the Afyon Kocatepe University 07-FENED.09 Project.

The author thanks B. Deveci, K. Kara, Durdu O. Guney, A. R. Boga, and T. T. Dermez, as well as Prof. Dr. Ö. E. Müstecaplıoğlu and S. Özen for their inspired communications.

References

1. J. Chiaverini and W. E. Lybarger Jr., *Phys. Rev. A*, **77**, 022324 (2008).
2. D. Leibfried, R. Blatt, C. Monroe, and D. Wineland, *Phys. Rev. Mod.*, **75**, 281 (2003).
3. M. Abdel-Aty and A. R. McGurn, *Phys. Lett. A*, **373**, 2420 (2009).

4. A. Einstein, B. Podolsky, and N. Rosen, *Phys. Rev.*, **47**, 777 (1935).
5. J. S. Bell, *Physics*, **1**, 195 (1964).
6. M. A. Can, O. Cakir, A. Klyachko, and A. Shumousky, *J. Opt. B: Quantum Semiclass. Opt.*, **6**, 513 (2004).
7. G. Gour and B. C. Senders, *Phys. Rev. Lett.*, **93**, 260501 (2004).
8. M. Abdel-Aty, *Opt. Commun.*, **266**, 225 (2006).
9. G. Gour, *Phys. Rev. A*, **72**, 042318 (2005).
10. Z. Ficek, *Appl. Math. Inform. Sci.*, **3**, 375 (2009).
11. A. El-Barakaty, M. Darwish, and A. S. F. Obada, *Appl. Math. Inform. Sci*, **5**, 122 (2011).
12. Li-Hui Sun, Gau-Xiang Li, and Z. Ficek, *Appl. Math. Inform. Sci.*, **4**, 315 (2010).
13. M. Sebawe Abdalla and L. Thabet, *Appl. Math. Inform. Sci.*, **5**, 570 (2011).
14. A.-H. M. Ahmed, M. N. Zakaria, and N. Metally, *Appl. Math. Inform. Sci.*, **3**, 375 (2009).
15. J. Maziero, L. C. Celeri, R. M. Serra, and M. S. Sarandy, *Phys. Lett. A*, **376**, 1540 (2012).
16. Jian-Song Zhang and Ai-Xi Chen, *Quantum Phys. Lett.*, **1**, 69 (2012).
17. A. B. A. Mohamed, *Quantum Inform. Rev.*, **1**, 1 (2013).
18. Bo Li, Zhi-Xi Wang, and Shao-Ming Fei, *Phys. Rev. A*, **83**, 022321 (2011).
19. R. Dermez and Ö. E. Müstecaplıoğlu, *Phys. Scr.*, **79**, 015304 (2009).
20. R. Dermez and S. Özen, *Eur. Phys. J. D*, **57**, 431 (2010).
21. C.-S. Yu and H.-S. Song, *Phys. Rev. A*, **73**, 022325 (2006).
22. R. Dermez and S. Özen, *Phys. Scr.*, **85**, 055009 (2012).
23. K. Berreda, M. El Baz, H. Eleuch, and Y. Hassouni, *Int. J. Mod. Phys. C*, **21**, 291 (2010).
24. K. Berreda, A. Benmoussa and Y. Hassouni, *Quantum Inform. Process.*, DOI 10.1007/s11128-010-0215-9 (2011).
25. I. J. Solomon, N. Mukunda, and R. Simon, *Quantum Inform. Process.*, DOI 10.1007/s11128-011-0316-0 (2011).
26. J. S. Kim, *Phys. Rev. A*, **80**, 022302 (2009).
27. D. C. Li and Z.-K. Shi, *Int. J. Theor. Phys.* **47**, 2645 (2008).
28. Z. Yu-Quing, T. Lei, Z. Zhong-Hua, et al., *Chinese Phys. B*, **19**, 024210 (2010).
29. Y. S. Myung, *Phys. Lett. B*, **636**, 324 (2006).
30. L. Borsten, *Nucl. Phys. B*, **216**, 218 (2011).
31. L. F. Wei, Y. Liu, and F. Nori, *Phys. Rev. A*, **70**, 063801 (2004).
32. Ö. E. Müstecaplıoğlu, *Phys. Rev. A*, **68**, 02381 (2003).
33. A. Ekert and P. L. Knight, *Amer. J. Phys.* **63**, 415 (1994).
34. M. Abdel-Aty, *J. Phys. B: At. Mol. Opt. Phys.*, **33**, 2665 (2000).
35. M. Abdel-Aty, *J. Phys. A: Math. Gen.* **38**, 8589 (2005).
36. Z.-J. Wang and F. Chen, *Chinese Phys. Lett.*, **24**, 1570 (2006).
37. C. Schmid, N. Kiesel, W. Wieczorek, and H. Weinfurter, *Phys. Rev. Lett.*, **101**, 260505 (2008).
38. H. Casini and M. Huerta, *Phys. Lett. B*, **694**, 167 (2010).
39. V. I. Man'ko and O. V. Man'ko, *J. Exp. Theor. Phys.*, **85**, 430 (1997).
40. M. A. Man'ko and V. I. Man'ko, and R. V. Mendes, *J. Russ. Laser Res.*, **27**, 507 (2006).
41. J. C. Retamal and N. Zagury, *Phys. Rev. A*, **55**, 2387 (1997).
42. O. Castaños, R. Jauregui, R. López-Peña, et al., *Phys. Rev. A*, **55**, 1208 (1997).
43. R. Dermez and S. Abdel-Khalek, *J. Russ. Laser Res.*, **32**, 287 (2011).
44. R. Dermez, S. A. Khalek, K. Kara K, et al., *J. Russ. Laser Res.*, **33**, 42 (2012).